Compact and Coding Expandable Chipless RFID Tag with Bending Arms

Hua Zhu [1,2], Xiuping Li [1,2], and Song Jia [1,2]

[1] School of Electronic Engineering
Beijing University of Posts and Telecommunications, Beijing, 100876, China

[2] Beijing Key Laboratory of Work Safety Intelligent Monitoring
Beijing University of Posts and Telecommunications, Beijing, 100876, China
judy-cool@163.com, xpli@bupt.edu.cn, 951684999@qq.com, xiaojun19861986@163.com

Abstract ─ In order to construct a compact chipless RFID tag with scalable coding capacity, a design is proposed that includes bending arms along both sides of the microstrip transmission line. Each bending arm produces a resonant frequency, which indicates one bit. And the bending structure can effectively reduce the coupling between units. A 12-bit chipless RFID tag with dimensions of 37×17.7mm^2 is designed with a frequency band from 5GHz to 6.05GHz. And a 40-bit chipless RFID tag is proposed with a frequency band from 2.95GHz to 5.65GHz. Both amplitude and Group Delay responses of the proposed tag are measured and analyzed. The measurement results are in good agreement with the simulation results. The measured results achieve stability and high capacity the coded information.

Index Terms ─ Chipless RFID tag, multi-stop band filter, resonant units.

I. INTRODUCTION

In recent years, the applications of radio frequency identification (RFID) are expanding exponentially in warehousing, supplied chain management and other automation processes due to penetrating ability and higher data transmission rate [1]. Although the traditional RFID systems based on the use of silicon RFID chips are very common and largely exploited in practice, some of their limitations, such as cost and robustness, are driving many researches towards alternative solutions, namely chipless RFID tag [2-3]. The most promising way for chipless RFID development is to directly print on product or package [4].

In general, a chipless RFID tag that utilizes frequency signature encoding consists of a vertically polarized UWB transmitting antenna, a horizontally polarized UWB receiving antenna and multi-resonant units, as shown in Figure 1. The cross-polarized antennas minimize cross talk between transmitting and receiving signal [5]. Overall, the receiving antenna is illuminated by the electromagnetic wave from the reader, and the signal from the receiving antenna is transmitted to the multi-resonant units to obtain multi-stopband or multi-passband filtering. The frequency band of operation is divided by N sections, corresponding to N bits. The presence and absence of resonance at each section of the frequency band is associated with bits '1' and '0', respectively. Research on chipless RFID tags can be broadly classified into two main categories: time domain reflectometry (TDR)-based chipless RFID tag [6-8], spectral signature-based chipless RFID tag [9-12] and amplitude/ phase backscatter modulation-based chipless RFID tag [13].

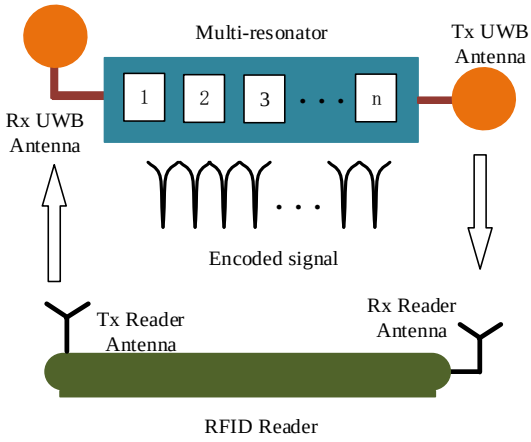

Fig. 1. Physical concept of the chipless RFID system.

Frequency-signature-based chipless RFID tag has a relatively high storage performance, which is an important feature in tag research. In [9], a 35-bit chipless RFID tag is designed with spiral resonance units. The tag operates between 3.1-7GHz. In [10], an 8-bit chipless RFID tag with eight E shape resonator units is proposed. The E shape resonators efficiently reduce coupling between units. However, the tag has low encoding density and the large dimension. In [11], an 8-bit chipless

Submitted On: June 28, 2018
Accepted On: May 12, 2019

RFID tag uses a split ring resonator unit that enhances the encoding capacity at a specific resonance frequency. In [12], 8-bit data encoded tag is proposed using multiple microstrip open stub resonators. In these researches, not only should the designed tag incorporate large amount of data, but should also be designed as compactly as possible. However, by increasing the number of bits on the tag, the couplings between the resonances are increased. Hence, the independence of the resonance frequency is reduced.

To overcome these problems, a 12-bit chipless RFID tag and a 40-bit chipless RFID tag with expandable coding capacity are designed and analyzed respectively in this paper. The chipless RFID tag consists of different bending arm units which are adopted to realize miniaturization and reduce the coupling between adjacent units.

II. DESIGN OF BENDING ARM ELEMENT

A. The resonant performance of the bending arm

To encode data within a frequency band, the design of a chipless RFID tag is combined with coupling filter technology, which is filtered through multiple resonant circuit units exited by a 50Ω microstrip transmission line. In this paper, the bending arms are loaded on both sides of the 50Ω microstrip transmission line to produce the multiple resonances and miniaturization, as shown in Fig. 2 (a). The yellow indicates metal and blue indicates the dielectric substrate. The bending arm consists of bends and lines, which is modeled by an equivalent T-network, as shown in Fig. 2 (b). Figure 2 (c) shows the simplified equivalent circuit which can be taken as a parallel circuit magnetically coupled to the main transmission line. Since the resonator unit is meandered, its equivalent inductance is increased, while the equivalent capacitance is slightly decreased [14]. This design assumes that the effective resistance of the bending arms can be ignored. The operating frequency f0 of the stop-band satisfies the following formula [13]:

$$f_0 = \frac{1}{2\pi} \frac{1}{\sqrt{\varepsilon_r \varepsilon_0 C_{Cs} (L_{Nm} + L_{T1} + M) \,||\, L_{Ns}}}, \qquad (1)$$

where M is the mutual inductance of L_{Nm} and L_{T1}.

The gap is a main parameter that affects M. When the value of gap is reduced, the mutual inductance M increases, and as a result the resonance frequency f_0 decreases judging by the equation (1). C_{Ns} is mainly generated by the value of h_1, which is the sum of the capacitance of the bending arm unit. L_{Ns} is the sum of the inductance value produced by a bending arm unit, which is affect by w_1. When the effective length of the bending arm element (w_1) is decreased, and then the L_{Ns} and C_{Ns} becomes smaller that results in the resonant frequency f_0 increases. When the parameter h_1 is decreased, the equivalent C_{Ns} decreases leading to the resonant frequency f_0 increases.

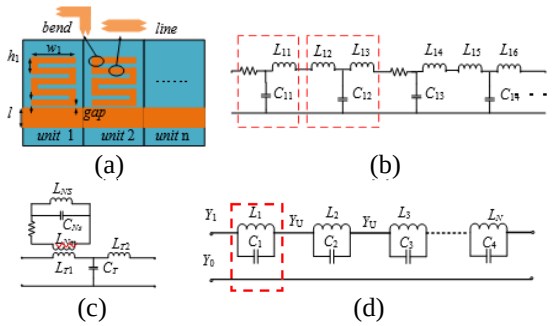

Fig. 2. The proposed chipless RFID structure and the equivalent circuit: (a) the proposed chipless RFID, (b) equivalent circuit of discrete element, (c) simplified equivalent circuit of bending arm unit, and (d) series parallel-resonant branches of N-bit chipless RFID tag.

Seen from the Fig. 3 (a), the center frequency of the bending arm unit is 5.07GHz with suitable band-stop filter characteristics. There is a significant in-band rejection using only 70MHz. The key parameters (w_1, h_1, *gap*) are simulated and analyzed, as shown in Figs. 2 (a-d). When the w_1 increases from 4mm to 6mm, the resonant frequency changes from 4.87GHz to 5.25GHz, as shown in Fig. 3 (b). Similarly, when the h_1 increases from 1.6mm to 2mm, the resonant frequency will shift from 5.55GHz to 4.63GHz in Fig. 3 (c). When the gap changes from 0.2mm to 0.5mm, the resonant frequency shifts from 5.02GHz to 5.12GHz, and the curve depth changes from -18.42dB to -11.04dB.

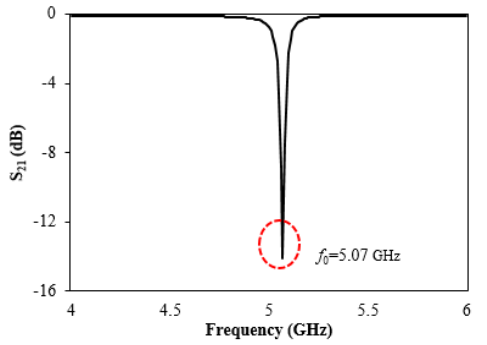

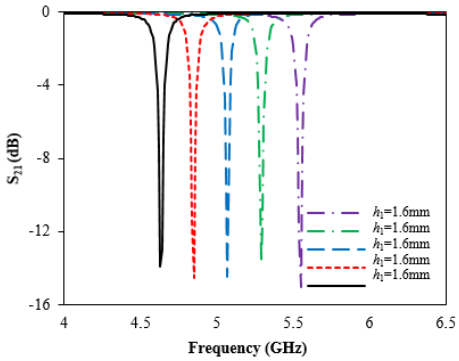

(c)

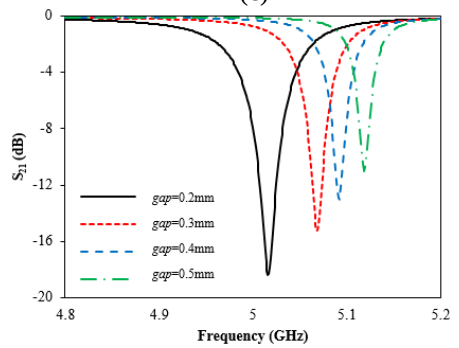

(d)

Fig. 3. Analysis of key parameters: (a) S_{21} of a single resonator, (b) S_{21} versus w_1, (c) S_{21} versus h_1, and (d) S_{21} versus *gap*.

B. The narrowband characteristic of the bending arm

In order to increase the number of codes at same bandwidth, the narrowband characteristic of the bending arm is required. The equivalent circuits for the multi-resonators of Fig. 2 (a) can be obtained as depicted in Fig. 2 (d), where Y_0 denote the terminating impedance and admittance. Consider a two-port network with a single series branch of $Y=j\omega C+1/j\omega L$, where L and C are the sum of inductance and the sum of capacitance.

The equation $\omega=\omega_0+\nabla\omega$, $\omega_0=1/\sqrt{LC}$, $b=\omega_0 C$ is substituted into the equation of Y:

$$\begin{aligned} Y &= j(\omega_0+\nabla\omega)\times C+\frac{1}{j(\omega_0+\nabla\omega)\times L} \\ &= j\omega_0 C+j\nabla\omega C+\frac{1}{j(\omega_0+\nabla\omega)}\times\omega_0^2 C \\ &= j\omega_0 C(1+\frac{\nabla\omega}{\omega_0}-\frac{\omega_0+\nabla\omega-\nabla\omega}{\omega_0+\nabla\omega}) \\ &\approx j\omega_0 C(1+\frac{\nabla\omega}{\omega_0}-1+\frac{\nabla\omega}{\omega_0}) \\ &= j\omega_0 C\times\frac{2\nabla\omega}{\omega_0} \end{aligned} \quad . \tag{2}$$

The transmission parameter with Y_0 is given by:

$$S_{21}=\frac{1}{1+\frac{Y_0}{2Y}}. \tag{3}$$

The equation (2) is substituted into the equation (3), and the S_{21} can be calculated as:

$$S_{21}=\frac{1}{1+\frac{Y_0}{2jb\frac{2\nabla\omega}{\omega_0}}}=\frac{1}{1-j\frac{Y_0}{4b\frac{\nabla\omega}{\omega_0}}}=\frac{1}{1-j\frac{1}{4\frac{b}{Y_0}}}\frac{\omega_0}{\nabla\omega}. \tag{4}$$

The amplitude of S_{21} can be calculated as:

$$|S_{21}|=\frac{1}{\sqrt{1+\left[\frac{\omega_0}{4(b/Y_0)\nabla\omega}\right]^2}}, \tag{5}$$

where a susceptance slope parameter $b=\omega_0 C=\frac{1}{\omega_0 L}$ and we can define the $|S_{21}|=m$dB .When the frequency shifts such as:

$$\frac{1}{4(b/Y_0)}\frac{\omega_0}{\nabla\omega_\pm}=\pm\sqrt{10^{\frac{m}{10}}-1}=\pm A, \tag{6}$$

the value of S_{21} will reach to $-m$dB. The mdB bandwidth can be defined by:

$$\nabla\omega_{mdB}=\nabla\omega_+-\nabla\omega_-=\frac{\omega_0}{4A(b/Y_0)}. \tag{7}$$

Therefore, we have:

$$\left(\frac{b}{Y_0}\right)=\frac{\omega_0}{4A\nabla\omega_{mdB}}=\frac{f_0}{4A\Delta f_{mdB}}, \tag{8}$$

$$\Delta f_{mdB}=\frac{Y_0}{8A\pi C}. \tag{9}$$

In conjunction with the preceding analysis, when the value of h_1 increases, the equivalent capacitance C increases leading to the bandwidth Δf_{mdB} decreases as shown in Fig. 3 (b). The performance of the designed chipless tag is simulated using the simulation tool HFSS. When the h_1 increases from 1.7mm to 2mm, the Δf_{3dB} shifts from 65.4MHz to 52.1MHz, and the Δf_{10dB} shifts from 20.4MHz to 14.6MHz. Similarly, when the *gap* increases, the equivalent capacitance C increases slightly, and the bandwidth Δf_{mdB} is decreased by equation (9), assuming that the frequency is constant. In Fig. 3 (d), when the *gap* increases from 0.2mm to 0.5mm, the Δf_{3dB} shifts from 76.5MHz to 29.4MHz, and the Δf_{10dB} shifts from 23.7MHz to 4.8MHz.

C. The coding independence of the bending arms

Furthermore, this is an efficient approach to encoding independently by reducing the coupling between the resonators. Figure 4 (a) shows the current distribution at 5.1GHz. The current is distributed mainly in the bending arm element along the x axis, while the current along the y axis is weak. Compared with the spiral structure [8], there is a strong current distribution along the direction of the x axis and y axis. When multiple units are arranged along with the transmission line, the coupling between adjacent units is reduced to achieve encoding independently. And the units' distance of proposed bending arm structure is 1mm for miniaturization,

compared the one of spiral structure (3mm). To sum up, the bending arm element provides the advantage of fully utilizing the frequency band without overlapping the resonant dips, and thus it prevents mutual coupling.

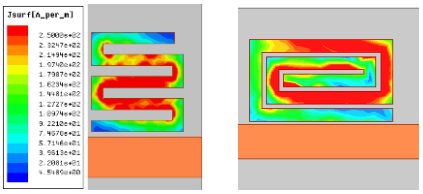

(a) (b)

Fig. 4. The current distribution at 5.1GHz: (a) bending arm structure, and (b) the spiral resonant units.

III. DESIGN OF CHIPLESS RFID TAG WITH BRNING ARMS

A. Design of the 12-bit chipless RFID tag

In the proposed chipless RFID tag, multi-resonance is achieved by adopting cascaded bending arm coupling to a 50Ω transmission microstrip line as shown in Fig. 5. The prototype is fabricated on a TXL-8 substrate (ε_r=2.55, h=0.787 mm, tanδ=0.0017) with dimensions of 37×17.7mm^2. The cascaded bending arms are distributed on both sides of 50Ω transmission line. The parameter for a 12-bit chipless RFID tag is shown in Table 1.

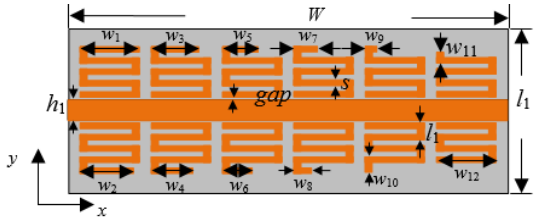

Fig. 5. Detail parameters of 12-bit chipless RFID tag.

Table 1: The optimal dimensions of the proposed 12-bit chipless RFID tag (Unit: mm)

Parameters	Value	Parameters	Value
L	17.7	w_5	3
W	37	w_6	2.5
h_1	2.2	w_7	2
s	0.6	w_8	1.5
l_1	1.8	w_9	1
w_0	5	w_{10}	1.7
w_1	5	w_{11}	1.2
w_2	4.5	w_{12}	0.7
w_3	4	gap	0.3
w_4	3.5	gap_1	1

The bending arm unit represents a logic state ‘1’ when interrogated with an incident wave. The logic state is changed to ‘0’ when the bending arm structure is removed or shortened. Each bending arm element with a different length contributes to a specific frequency. The removed bending arm unit will show no resonance in our desired band, and thus absence of a resonance dip corresponds to a 0-bit at the respective resonance frequency. Incorporating this concept, numerous tag IDs can be generated by removing or keeping different units, as shown in Fig. 6.

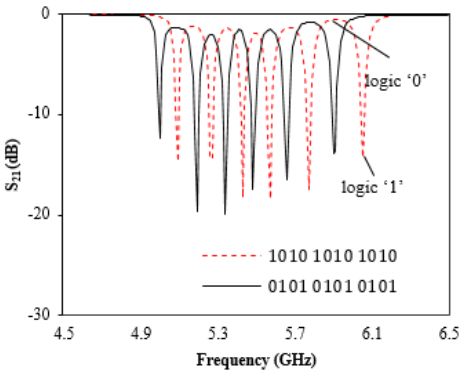

Fig. 6. The simulated result of bit combination ‘1010 1010 1010’ and ‘0101 0101 0101’.

Therefore, a unique ID can be allocated to each tag which results in avoiding the collision of data in any network. There is a code for ‘0101 0101 0101’ when the six resonant units above the transmission line is removed. Similarly, the six bending resonant units loaded below the transmission line are removed, and the code of ‘1010 1010 1010’ is achieved. Comparing the two sets of codes, it can be seen that two cases of coding frequency points are interspersed with each other, generating the code of ‘1111 1111 1111’. The coding works in the bandwidth of 5-6.04GHz, and each code occupies 88MHz.

Figure 7 shows surface current at 5.00GHz, 5.10GHz, 5.44GHz, and 5.91GHz. When the operating frequency is 5GHz, it implies the current distribution of the first bending arm element is strongest. And so as the other frequencies.

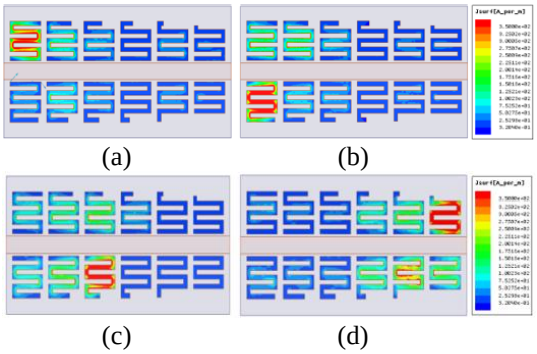

(a) (b)

(c) (d)

Fig. 7. Surface current distributions: (a) 5.00GHz, (b) 5.10GHz, (c) 5.44GHz, and (d) 5.91GHz.

B. Design of the 40-bit chipless RFID tag

To expand the coding capacity, a 40-bit chipless tag, which can reserve 240 data, is proposed. The 40-bit chipless RFID tag consists of 40 bending resonators and a transmission line, with dimension of 146.8×29.7mm^2, as shown in Fig. 8. In addition, each bending arm element responds to a specific resonant frequency.

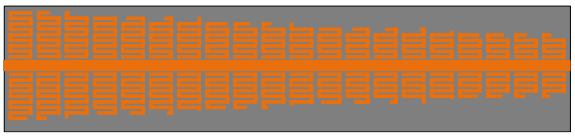

Fig. 8. A 40-bit chipless RFID tag.

Figure 9 shows the results of transmission coefficient and Group Delay for the 40-bit chipless RFID tag, which operates between 2.95GHz and 5.65GHz, occupying just 67.5MHz for each bit. Keeping the bending arm units above or below the transmission line respectively, the two kinds of codes are interspersed into each other, as shown in Fig. 10.

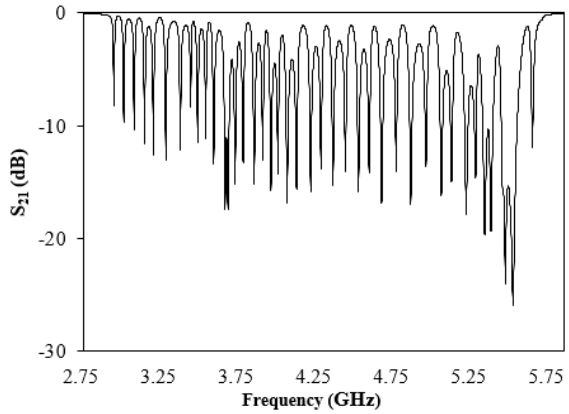

(a)

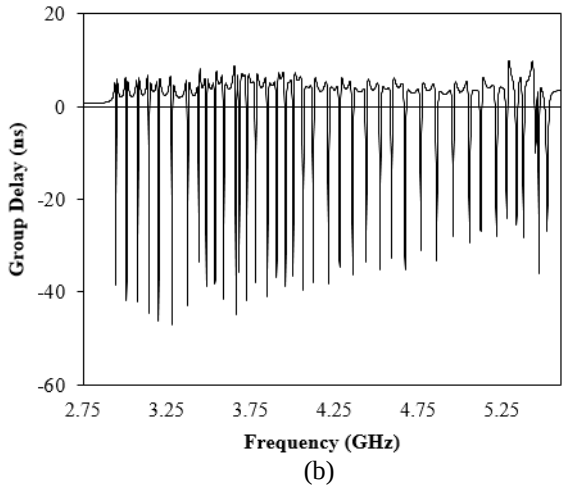

(b)

Fig. 9. Simulated results for 40-bit chipless RFID tag: (a) transmission characters, and (b) group delay.

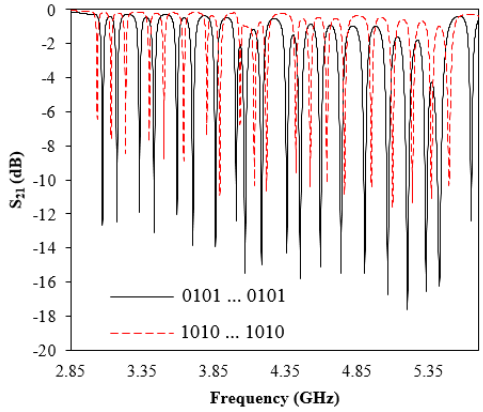

(a)

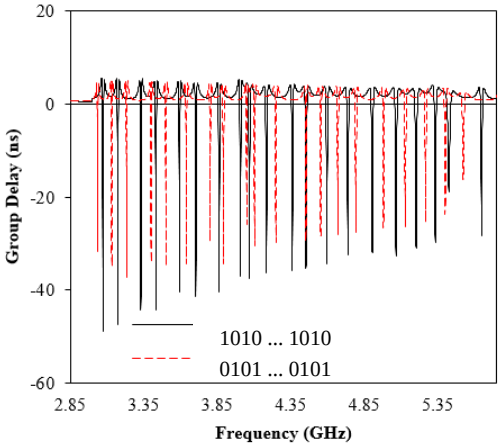

(b)

Fig. 10. Simulated results for 40-bit chipless RFID tag with different data: (a) transmission character, and (b) group delay.

IV. FABRICATION AND RESULTS

Figure 11 (a) shows photograph of the designed 12 bending arm units. The S_{21} and group delay is measured by vector network analyzer (VNA) connected to both ends of proposed 12-bit chipless RFID tag, as shown in Fig. 11 (b). Each bending arm unit has a 1:1 correspondence with a data bit (12 units=12 bits).

As shown in Fig. 12, the simulated bandwidth of the proposed 12-bit chipless RFID tag is from 5GHz to 6.05GHz, while the measured one is from 4.99GHz to 6.04GHz. And each of the bits occupies 87.5 MHz on average. Moreover, the measured data points show close correspondence with the simulated results with twelve different resonance points operating at the frequencies of 5.00GHz, 5.08GHz, 5.18GHz, 5.30GHz, 5.38GHz, 5.44GHz, 5.53GHz, 5.60GHz, 5.69GHz, 5.71GHz, 5.79GHz, 5.91GHz and 6.03GHz. It is clear that there is a small shift in the resonant frequency due to mutual coupling effect between the resonators. The band notches are well defined and for the worst case the magnitude of the dip is better than 5 dB.

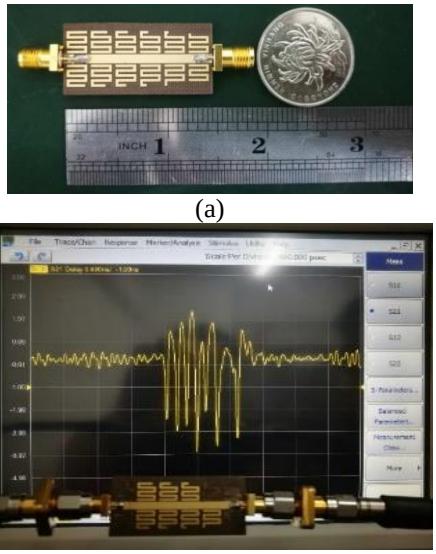

Fig. 11. Photo of the measurement environment: (a) fabrication of the 12-bit chipless RFID tag, and (b) experimental set up for bistatic measurement.

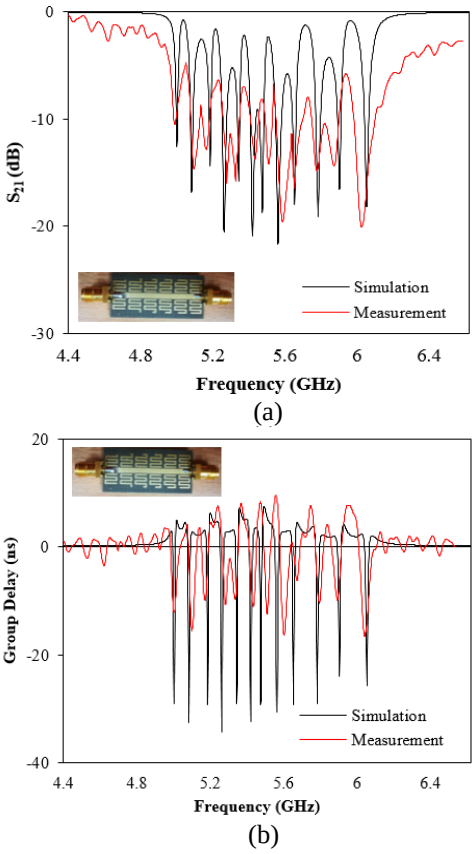

Fig. 12. Measured and simulated S_{21} results of proposed chipless RFID tag: (a) S_{21} result of the bit '1111 1111 1111', and (b) group delay result of the bit '1111 1111 1111'.

The performance comparison of the proposed and other reported chipless RFID tags are listed in Table 2. The proposed chipless tag with bending arms in this article has higher coding density and narrower inter-code bandwidth.

Table 2: Performance comparison of the proposed RFID chipless tags and references

	Dimensions (mm^3)	**Frequency (GHz)**	**Bandwidth/bit (MHz)**	**Capacity (bit)**
Work 1	37×17.7	1.09 (5.0-6.05)	87.5	12
Work 2	146.8×29.7	2.7 (2.95-5.65)	67.5	40
[9]	88×65	3.9 (3.1-7.0)	111.4	35
[10]	59×30	0.65 (3.12-3.77)	81.25	8
[11]	25×50	4 (3.4-7.4)	500	8
[12]	50×30	2.6 (1.9-4.5)	420	8

V. CONCLUSION

In this paper, a novel chipless RFID tag with bending arm units is presented. Each bending arm unit produces a resonant frequency that indicates one bit. The proposed tag not only enhanced the data capacity within the minimum frequency area, but also improved the isolation and density. A 12-bit RFID chipless tag is simulated and measured. A 40-bit chipless tag is simulated and analyzed. The simulated and measured results agree well.

ACKNOWLEDGMENT

This work is supported by the Fundamental Research Funds for the Central Universities.

REFERENCES

[1] X. Li, H. Zhu, D. Zhang, Z. Sun, Y. Yuan, and D. Yu, "Two-dimensional scanning antenna array for UHF radio frequency identification system application," *IET Microwaves, Antennas & Propagation*, vol. 8, no. 14, pp. 1250-1258, 2014.

[2] M. M. Khan, F. A. Tahir, M. F. Farooqui, A. Shamim, and H. M. Cheema, "3.56-bits/cm^2 compact inkjet printed and application specific chipless RFID tag," *IEEE Antennas and Wireless Propagation Letters*, vol. 15, pp. 1109-1112, 2016.

[3] Md. A. Islam and N. C. Karmakar, "A 4×4 dual polarized mm-wave ACMPA array for a universal mm-wave chipless RFID tag reader," *IEEE Transactions on Antennas and Propagation*, vol. 63, no. 4, pp. 1633-1640, 2015.

[4] A. Vena, E. Perret, and S. Tedjini, "A fully printable chipless RFID tag with detuning

correction technique," *IEEE Microwave and Wireless Components Letters*, vol. 22, no. 4, pp. 209-211, 2012.

[5] S. Preradovic and N. C. Karmakar, "Design of fully printable planar chipless RFID transponder with 35-bit data capacity," *Proceedings of the 39th European Microwave Conference*.

[6] A. Ramos, A. Lazaro, D. Girbau, et al., "Time-domain measurement of time-coded UWB chipless RFID tags," *Progress in Electromagnetics Research*, vol. 116, no. 8, pp. 313-331, 2011.

[7] M. Pöpperl, A. Parr, C. Mandel, R. Jakoby, and M. Vossiek, "Potential and practical limits of time-domain reflectometry chipless RFID," *IEEE Transactions on Microwave Theory & Techniques*, pp. 1-9, 2016.

[8] D. Girbau, Á. Ramos, A. Lazaro, and R. Villarino, "Passive wireless temperature sensor based on time-coded UWB chipless RFID tags," *IEEE Transactions on Microwave Theory & Techniques*, vol. 60, no. 11, pp. 3623-3632, 2012.

[9] S. Preradovic, I. Balbin, N. C. Karmakar, and G. F. Swiegers, "Multiresonator-based chipless RFID system for low-cost item tracking," *IEEE Transactions on Microwave Theory and Technique*, vol. 57, no. 5, pp. 1411-1419, 2009.

[10] M. Sumi, R. Dinesh, C. M. Nijas, S. Mridula, and P. Mohanan, "High bit encoding chipless RFID tag using multiple E-shaped microstrip resonators," *Progress In Electromagnetics Research B*, vol. 61, pp. 185-196, 2014.

[11] M. E. Jalil, M. K. A. Rahim, N. A. Samsuri, and R. Dewan, "Flexible printed chipless RFID tag using metamaterial-split ring resonator," *Applied Physics A*, pp. 122:348, 2016.

[12] C. M. Nijas, R. Dinesh, U. Deepak, A. Rasheed, S. Mridula, K. Vasudevan, and P. Mohanan, "Chipless RFID tag using multiple microstrip open stub resonators," *IEEE Transactions on Antennas and Propagation*, vol. 60, no. 9, pp. 4429-4432, Sept. 2012.

[13] E. Md. Amin, Md. S. Bhuiyan, N. C. Karmakar, and B. Winther-Jensen, "Development of a low cost printable chipless RFID humidity sensor," *IEEE Sensors Journal*, vol. 14, no. 1, pp. 140-149, 2014.

[14] C. M. Nijas, U. Deepak, P. V. Vinesh, and R. Sujith, "Low-cost multiple-bit encoded chipless RFID tag using stepped impedance resonator," *IEEE Transactions on Antennas and Propagation*, vol. 62, no. 9, pp. 4762-4770, 2014.

Hua Zhu received the M. S. degree from Guilin University of Electronic Technology, P. R. China, in 2010, and the Ph.D. degree from Beijing Institute of Technology, Beijing, P. R. China, in 2015. She has been a postdoc at Beijing University of Posts and Telecommunications, P. R. China.

Her research interests include UHF RFID beam scanning antenna array design in complex environment and millimeter wave/ Terahertz antenna design.

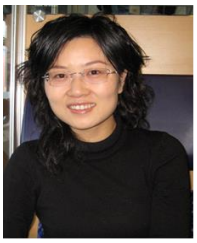

Xiuping Li received the B. S. degree from Shandong University, Jinan, Shandong, P. R. China, in 1996, and the Ph.D. degree from Beijing Institute of Technology, Beijing, P. R. China, in 2001. She has been a professor at Beijing University of Posts and Telecommunications, P. R. China.

Her research interests include microwave devices for communications, antennas, and microwave circuit design for millimeter wave/ Terahertz applications.

Jia Song received the B.S. degree from Chongqing University of Posts and Telecommunications, P. R. China, in 2013, and the M.S. degree from Beijing University of Posts and Telecommunications, P. R. China, in 2016.

Her research interests include chipless RFID techniques.